

000 054  
 001 055  
 002 056  
 003 057  
 004 058  
 005 059  
 006 060  
 007 061  
 008 062  
 009 063  
 010 064  
 011 065  
 012 066  
 013 067  
 014 068  
 015 069  
 016 070  
 017 071  
 018 072  
 019 073  
 020 074  
 021 075  
 022 076  
 023 077  
 024 078  
 025 079  
 026 080  
 027 081  
 028 082  
 029 083  
 030 084  
 031 085  
 032 086  
 033 087  
 034 088  
 035 089  
 036 090  
 037 091  
 038 092  
 039 093  
 040 094  
 041 095  
 042 096  
 043 097  
 044 098  
 045 099  
 046 100  
 047 101  
 048 102  
 049 103  
 050 104  
 051 105  
 052 106  
 053 107

## Supplementary Materials to ‘‘Multi-channel Weighted Nuclear Norm Minimization for Real Color Image Denoising’’

Anonymous ICCV submission

Paper ID 572

In this supplementary file, we provide:

1. The proof of the Theorem 1 in the main paper;
2. More denoising results on the Kodak PhotoCD dataset;
3. More visual comparisons of denoised images on the real noisy images of dataset [1];
4. More visual comparisons of denoised images on the real noisy images of dataset [2].

### 1. Proof of Theorem 1.

**Theorem 1.** Assume that the weights in  $w$  are in a non-descending order, the sequence  $\{\mathbf{X}_k\}$ ,  $\{\mathbf{Z}_k\}$ , and  $\{\mathbf{A}_k\}$  generated in Algorithm 1 satisfy:

$$(a) \lim_{k \rightarrow \infty} \|\mathbf{X}_{k+1} - \mathbf{Z}_{k+1}\|_F = 0; \quad (b) \lim_{k \rightarrow \infty} \|\mathbf{X}_{k+1} - \mathbf{X}_k\|_F = 0; \quad (c) \lim_{k \rightarrow \infty} \|\mathbf{Z}_{k+1} - \mathbf{Z}_k\|_F = 0. \quad (1)$$

*Proof.* 1. Firstly, we prove that the sequence  $\{\mathbf{A}_k\}$  generated by Algorithm 1 is upper bounded. Let  $\mathbf{X}_{k+1} + \rho_k^{-1} \mathbf{A}_k = \mathbf{U}_k \Sigma_k \mathbf{V}_k^\top$  be its singular value decomposition (SVD) [3] in the  $(k+1)$ -th iteration. According to Corollary 1 of [4], we can have the SVD of  $\mathbf{Z}_{k+1}$  as  $\mathbf{Z}_{k+1} = \mathbf{U}_k \hat{\Sigma}_k \mathbf{V}_k^\top = \mathbf{U}_k \mathcal{S}_{\frac{w}{\rho_k}}(\Sigma_k) \mathbf{V}_k^\top$ . Then we have

$$\|\mathbf{A}_{k+1}\|_F = \|\mathbf{A}_k + \rho_k(\mathbf{X}_{k+1} - \mathbf{Z}_{k+1})\|_F = \rho_k \|\rho_k^{-1} \mathbf{A}_k + \mathbf{X}_{k+1} - \mathbf{Z}_{k+1}\|_F \quad (2)$$

$$= \rho_k \|\mathbf{U}_k \Sigma_k \mathbf{V}_k^\top - \mathbf{U}_k \mathcal{S}_{\frac{w}{\rho_k}}(\Sigma_k) \mathbf{V}_k^\top\|_F = \rho_k \|\Sigma_k - \mathcal{S}_{\frac{w}{\rho_k}}(\Sigma_k)\|_F \quad (3)$$

$$= \rho_k \sqrt{\sum_i (\Sigma_k^{ii} - \mathcal{S}_{\frac{w}{\rho_k}}(\Sigma_k^{ii}))^2} \leq \rho_k \sqrt{\sum_i (\frac{w_i}{\rho_k})^2} = \sqrt{\sum_i w_i^2}. \quad (4)$$

The inequality in the second last step can be proved as follows: given the diagonal matrix  $\Sigma_k$ , we define  $\Sigma_k^{ii}$  as the  $i$ -th element of  $\Sigma_k^{ii}$ . If  $\Sigma_k^{ii} \geq \frac{w_i}{\rho_k}$ , we have  $\mathcal{S}_{\frac{w}{\rho_k}}(\Sigma_k^{ii}) = \Sigma_k^{ii} - \frac{w_i}{\rho_k}$ . If  $\Sigma_k^{ii} < \frac{w_i}{\rho_k}$ , we have  $\mathcal{S}_{\frac{w}{\rho_k}}(\Sigma_k^{ii}) = 0$ . Overall, we have  $|\Sigma_k^{ii} - \mathcal{S}_{\frac{w}{\rho_k}}(\Sigma_k^{ii})| \leq \frac{w_i}{\rho_k}$  and hence the inequality holds. Hence, the sequence  $\{\mathbf{A}_k\}$  is upper bounded.

2. Secondly, we prove that the sequence of Lagrangian function  $\{\mathcal{L}(\mathbf{X}_{k+1}, \mathbf{Z}_{k+1}, \mathbf{A}_k, \rho_k)\}$  is also upper bounded. Since we have the globally optimal solution of  $\mathbf{X}$  and  $\mathbf{Z}$  in their corresponding subproblems, we always have

$$\mathcal{L}(\mathbf{X}_{k+1}, \mathbf{Z}_{k+1}, \mathbf{A}_k, \rho_k) \leq \mathcal{L}(\mathbf{X}_k, \mathbf{Z}_k, \mathbf{A}_k, \rho_k). \quad (5)$$

Based on the updating rule that  $\mathbf{A}_{k+1} = \mathbf{A}_k + \rho_k(\mathbf{X}_{k+1} - \mathbf{Z}_{k+1})$ , we have

$$\mathcal{L}(\mathbf{X}_{k+1}, \mathbf{Z}_{k+1}, \mathbf{A}_{k+1}, \rho_{k+1}) \quad (6)$$

$$= \mathcal{L}(\mathbf{X}_{k+1}, \mathbf{Z}_{k+1}, \mathbf{A}_k, \rho_k) + \langle \mathbf{A}_{k+1} - \mathbf{A}_k, \mathbf{X}_{k+1} - \mathbf{Z}_{k+1} \rangle + \frac{\rho_{k+1} - \rho_k}{2} \|\mathbf{X}_{k+1} - \mathbf{Z}_{k+1}\|_F^2 \quad (7)$$

$$= \mathcal{L}(\mathbf{X}_{k+1}, \mathbf{Z}_{k+1}, \mathbf{A}_k, \rho_k) + \frac{\rho_{k+1} + \rho_k}{2\rho_k^2} \|\mathbf{A}_{k+1} - \mathbf{A}_k\|_F^2. \quad (8)$$

108 Since the sequence  $\{\mathbf{A}_k\}$  is upper bounded, the sequence  $\{\mathbf{A}_{k+1} - \mathbf{A}_k\}$  is also upper bounded. Denote by  $a$  the upper bound  
 109 of  $\{\mathbf{A}_{k+1} - \mathbf{A}_k\}$ , i.e.,  $\|\mathbf{A}_{k+1} - \mathbf{A}_k\|_F \leq a$  holds for  $\forall k \geq 0$ , we have  
 110

$$\begin{aligned} 111 \quad \mathcal{L}(\mathbf{X}_{k+1}, \mathbf{Z}_{k+1}, \mathbf{A}_{k+1}, \rho_{k+1}) &\leq \mathcal{L}(\mathbf{X}_1, \mathbf{Z}_1, \mathbf{A}_0, \rho_0) + a^2 \sum_{k=0}^{\infty} \frac{\rho_{k+1} + \rho_k}{2\rho_k^2} \\ 112 \end{aligned} \quad (9)$$

$$\begin{aligned} 113 \quad &= \mathcal{L}(\mathbf{X}_1, \mathbf{Z}_1, \mathbf{A}_0, \rho_0) + a^2 \sum_{k=0}^{\infty} \frac{\mu + 1}{2\mu^k \rho_0} \\ 114 \end{aligned} \quad (10)$$

$$\begin{aligned} 115 \quad &\leq \mathcal{L}(\mathbf{X}_1, \mathbf{Z}_1, \mathbf{A}_0, \rho_0) + \frac{a^2}{\rho_0} \sum_{k=0}^{\infty} \frac{1}{\mu^{k-1}}. \\ 116 \end{aligned} \quad (11)$$

117 The last inequality holds since  $\mu > 1$  and  $\mu + 1 < 2\mu$ . Therefore, we have  $\sum_{k=0}^{\infty} \frac{1}{\mu^{k-1}} < \infty$  and the sequence of Lagrangian  
 118 function  $\{\mathcal{L}(\mathbf{X}_{k+1}, \mathbf{Z}_{k+1}, \mathbf{A}_{k+1}, \rho_{k+1})\}$  is upper bounded.  
 119

120 3. Thirdly, we prove that the sequences of  $\{\mathbf{X}_k\}$  and  $\{\mathbf{Z}_k\}$  are upper bounded. Since  
 121

$$\begin{aligned} 122 \quad \|\mathbf{W}(\mathbf{Y} - \mathbf{X}_k)\|_F^2 + \|\mathbf{Z}_k\|_{\mathbf{w},*} = \mathcal{L}(\mathbf{X}_k, \mathbf{Z}_k, \mathbf{A}_{k-1}, \rho_{k-1}) - \langle \mathbf{A}_k, \mathbf{X}_k - \mathbf{Z}_k \rangle - \frac{\rho_k}{2} \|\mathbf{X}_k - \mathbf{Z}_k\|_F^2 \\ 123 \end{aligned} \quad (12)$$

$$\begin{aligned} 124 \quad &= \mathcal{L}(\mathbf{X}_k, \mathbf{Z}_k, \mathbf{A}_{k-1}, \rho_{k-1}) + \frac{1}{2\rho_k} (\|\mathbf{A}_{k-1}\|_F^2 - \|\mathbf{A}_k\|_F^2), \\ 125 \end{aligned} \quad (13)$$

126 both  $\{\mathbf{W}(\mathbf{Y} - \mathbf{X}_k)\}$  and  $\{\mathbf{Z}_k\}$  are upper bounded, and hence the sequence  $\{\mathbf{X}_k\}$  is bounded by the Cauchy-Schwarz  
 127 inequality and triangle inequality. We can obtain that  
 128

$$\lim_{k \rightarrow \infty} \|\mathbf{X}_{k+1} - \mathbf{Z}_{k+1}\|_F = \lim_{k \rightarrow \infty} \rho_k^{-1} \|\mathbf{A}_{k+1} - \mathbf{A}_k\|_F = 0, \quad (14)$$

129 and the equation (a) is proved.  
 130

131 4. Then we can prove that

$$\begin{aligned} 132 \quad \lim_{k \rightarrow \infty} \|\mathbf{X}_{k+1} - \mathbf{X}_k\|_F &= \lim_{k \rightarrow \infty} \|(\mathbf{W}^\top \mathbf{W} + \frac{\rho_k}{2} \mathbf{I})^{-1} (\mathbf{W}^\top \mathbf{W} \mathbf{Y} - \mathbf{W}^\top \mathbf{W} \mathbf{Z}_k - \frac{1}{2} \mathbf{A}_k) - \rho_k^{-1} (\mathbf{A}_k - \mathbf{A}_{k-1})\|_F \\ 133 \end{aligned} \quad (15)$$

$$\begin{aligned} 134 \quad &\leq \lim_{k \rightarrow \infty} \|(\mathbf{W}^\top \mathbf{W} + \frac{\rho_k}{2} \mathbf{I})^{-1} (\mathbf{W}^\top \mathbf{W} \mathbf{Y} - \mathbf{W}^\top \mathbf{W} \mathbf{Z}_k - \frac{1}{2} \mathbf{A}_k)\|_F + \rho_k^{-1} \|\mathbf{A}_k - \mathbf{A}_{k-1}\|_F \\ 135 \end{aligned} \quad (16)$$

$$= 0, \quad (17)$$

136 and hence the equation (b) is proved.  
 137

138 5. Finally, the equation (c) can be proved by checking that

$$\begin{aligned} 139 \quad \lim_{k \rightarrow \infty} \|\mathbf{Z}_{k+1} - \mathbf{Z}_k\|_F &= \lim_{k \rightarrow \infty} \|\mathbf{X}_k + \rho_k^{-1} \mathbf{A}_{k-1} - \mathbf{Z}_k + \mathbf{X}_{k+1} - \mathbf{X}_k + \rho_k^{-1} \mathbf{A}_{k-1} + \rho_k^{-1} \mathbf{A}_k - \rho_k^{-1} \mathbf{A}_{k+1}\|_F \\ 140 \end{aligned} \quad (18)$$

$$\leq \lim_{k \rightarrow \infty} (\|\Sigma_{k-1} - \mathcal{S}_{\mathbf{w}/\rho_{k-1}}(\Sigma_{k-1})\|_F + \|\mathbf{X}_{k+1} - \mathbf{X}_k\|_F + \rho_k^{-1} \|\mathbf{A}_{k-1} + \mathbf{A}_{k+1} - \mathbf{A}_k\|_F) \quad (19)$$

$$\leq \lim_{k \rightarrow \infty} (\rho_{k-1}^{-1} \|\mathbf{w}\|_F + \|\mathbf{X}_{k+1} - \mathbf{X}_k\|_F + \rho_k^{-1} \|\mathbf{A}_{k-1} + \mathbf{A}_{k+1} - \mathbf{A}_k\|_F) \quad (20)$$

$$= 0, \quad (21)$$

141 where  $\mathbf{U}_{k-1} \Sigma_{k-1} \mathbf{V}_{k-1}^\top$  is the SVD of the matrix  $\mathbf{X}_k + \rho_{k-1} \mathbf{A}_{k-1}$ . □  
 142

143

## 144 2. More denoising results on the Kodak PhotoCD dataset

145 In the main paper, we have given the PSNR results of the competing methods on the 24 high quality images from the  
 146 Kodak PhotoCD dataset when the standard deviations of the additive white Gaussian noise (AWGN) are  $\sigma_r = 40, \sigma_g = 20, \sigma_b = 30$  for R, G, B channels, respectively. Here we provide more denoising results on this dataset. In Tables 1-3,  
 147 we give the PSNR results on these images when the noise standard deviations are  $\sigma_r = 40, \sigma_g = 20, \sigma_b = 30$  in Table 1,  
 148  $\sigma_r = 30, \sigma_g = 10, \sigma_b = 50$  in Table 2 and  $\sigma_r = 5, \sigma_g = 30, \sigma_b = 15$  in Table 3, respectively. In Figures 1-6, we give the  
 149 visual comparisons of the denoised images by different methods.  
 150

151

152

153

154

155

156

157

158

159

160

161

Table 1. PSNR(dB) results of different denoising methods on the Kodak PhotoCD dataset.

Image#	$\sigma_r = 40, \sigma_g = 20, \sigma_b = 30$								
	CBM3D	MLP	TNRD	NI	NC	WNNM-1	WNNM-2	WNNM-3	MC-WNNM
1	25.24	25.70	25.74	23.85	24.90	26.01	25.95	25.58	<b>26.66</b>
2	28.27	30.12	30.21	25.90	25.87	30.08	30.11	29.80	<b>30.20</b>
3	28.81	31.19	31.49	26.00	28.58	31.58	31.61	31.20	<b>32.25</b>
4	27.95	29.88	29.86	25.82	25.67	30.13	30.16	29.84	<b>30.49</b>
5	25.03	26.00	26.18	24.38	25.15	26.44	26.39	25.32	<b>26.82</b>
6	26.24	26.84	26.90	24.65	24.74	27.39	27.30	26.88	<b>27.98</b>
7	27.88	30.28	30.40	25.63	27.69	30.47	30.54	29.70	<b>30.98</b>
8	25.05	25.59	25.83	24.02	25.30	26.71	26.75	25.26	<b>26.90</b>
9	28.44	30.75	30.81	25.94	27.44	30.86	30.92	30.29	<b>31.49</b>
10	28.27	30.38	30.57	25.87	28.42	30.65	30.68	29.95	<b>31.26</b>
11	26.95	28.00	28.14	25.32	24.67	28.19	28.16	27.61	<b>28.63</b>
12	28.76	30.87	31.05	26.01	28.37	30.97	31.06	30.58	<b>31.48</b>
13	23.76	23.95	23.99	23.53	22.76	24.27	24.15	23.52	<b>24.89</b>
14	26.02	26.97	27.11	24.94	25.68	27.20	27.15	26.55	<b>27.57</b>
15	28.38	30.15	30.44	26.06	28.21	30.52	30.60	30.13	<b>30.81</b>
16	27.75	28.82	28.87	25.69	26.66	29.27	29.21	29.02	<b>29.96</b>
17	27.90	29.57	29.80	25.85	28.32	29.78	29.79	29.16	<b>30.40</b>
18	25.77	26.40	26.41	24.74	25.70	26.63	26.56	26.01	<b>27.22</b>
19	27.30	28.67	28.81	25.40	26.52	29.19	29.22	28.67	<b>29.57</b>
20	28.96	30.40	30.76	24.95	25.90	30.79	30.83	29.97	<b>31.07</b>
21	26.54	27.53	27.60	25.06	26.48	27.80	27.75	27.12	<b>28.34</b>
22	27.05	28.17	28.27	25.36	26.60	28.21	28.16	27.81	<b>28.64</b>
23	29.14	32.31	32.51	26.13	23.24	31.89	31.97	31.21	<b>32.34</b>
24	25.75	26.41	26.53	24.55	25.73	27.10	27.03	26.18	<b>27.59</b>
<b>Average</b>	27.13	28.54	28.68	25.24	26.19	28.84	28.83	28.22	<b>29.31</b>

Table 2. PSNR(dB) results of different denoising methods on the Kodak PhotoCD dataset.

Image#	$\sigma_r = 30, \sigma_g = 10, \sigma_b = 50$								
	CBM3D	MLP	TNRD	NI	NC	WNNM-1	WNNM-2	WNNM-3	MC-WNNM
1	23.38	26.49	26.50	24.82	23.59	26.40	25.60	24.76	<b>27.81</b>
2	25.19	30.94	30.90	26.82	27.79	30.89	29.75	29.21	<b>30.96</b>
3	25.39	32.03	32.09	27.52	27.41	32.20	31.17	30.39	<b>32.89</b>
4	24.96	30.55	30.47	27.34	27.00	30.74	29.71	29.10	<b>31.19</b>
5	23.29	26.65	26.73	25.72	26.67	26.74	25.98	24.68	<b>27.60</b>
6	24.09	27.76	27.70	26.10	26.12	27.85	26.96	26.01	<b>29.15</b>
7	24.89	30.70	30.72	27.17	28.07	30.91	29.94	28.87	<b>31.37</b>
8	23.30	26.12	26.27	25.59	26.11	26.87	26.33	24.74	<b>27.44</b>
9	25.20	31.35	31.31	27.74	28.33	31.30	30.45	29.44	<b>32.08</b>
10	25.13	31.01	31.05	27.60	28.53	31.12	30.17	29.21	<b>31.83</b>
11	24.54	28.79	28.82	26.72	24.40	28.73	27.79	26.94	<b>29.60</b>
12	25.43	31.60	31.60	27.82	29.01	31.59	30.62	29.91	<b>32.11</b>
13	22.50	24.71	24.73	24.96	23.36	24.70	23.85	22.86	<b>25.96</b>
14	23.91	27.69	27.72	26.26	23.08	27.62	26.81	25.91	<b>28.57</b>
15	25.45	31.09	31.05	27.36	28.49	31.29	30.21	29.46	<b>31.39</b>
16	24.89	29.79	29.73	27.35	27.10	29.84	28.85	28.13	<b>31.10</b>
17	25.12	30.26	30.24	27.15	27.54	30.11	29.35	28.43	<b>31.08</b>
18	23.83	27.26	27.26	26.05	26.15	27.32	26.18	25.28	<b>28.32</b>
19	24.63	29.40	29.39	27.06	27.41	29.78	28.87	28.05	<b>30.53</b>
20	26.43	31.16	31.27	26.43	26.92	31.25	30.43	29.41	<b>31.55</b>
21	24.24	28.26	28.27	26.66	27.18	28.22	27.45	26.40	<b>29.29</b>
22	24.51	29.03	29.06	26.83	27.64	29.02	27.81	27.18	<b>29.57</b>
23	25.55	32.87	32.75	27.60	23.75	32.58	31.46	30.50	<b>32.34</b>
24	23.85	27.06	27.13	25.86	27.05	27.50	26.63	25.55	<b>28.32</b>
<b>Average</b>	24.57	29.27	29.28	26.69	26.61	29.36	28.43	27.52	<b>30.09</b>

324 Table 3. PSNR(dB) results of different denoising methods on the Kodak PhotoCD dataset. 378  
325  $\sigma_r = 5, \sigma_g = 30, \sigma_b = 15$  39

Image#	CBM3D	MLP	TNRD	NI	NC	WNNM-1	WNNM-2	WNNM-3	MC-WNNM
1	27.25	28.06	28.62	25.00	29.55	28.16	27.95	28.15	<b>30.20</b>
2	29.70	31.30	32.70	27.80	29.69	32.54	31.60	31.73	<b>34.04</b>
3	30.34	31.98	34.07	28.02	31.93	33.91	33.68	33.52	<b>35.55</b>
4	29.47	31.10	32.56	27.70	32.56	32.68	31.85	31.90	<b>34.06</b>
5	27.31	28.59	29.35	26.14	30.00	28.83	29.00	28.91	<b>30.05</b>
6	28.20	29.10	29.90	26.15	28.81	29.55	29.46	29.62	<b>31.64</b>
7	29.73	31.60	33.46	27.22	31.63	33.09	33.29	32.86	<b>34.24</b>
8	27.47	28.16	28.91	25.34	30.16	29.15	29.24	29.03	<b>29.91</b>
9	30.07	31.63	33.55	27.86	31.54	33.19	33.20	32.95	<b>34.53</b>
10	29.96	31.37	33.20	27.74	33.44	32.98	33.02	32.74	<b>34.38</b>
11	28.73	29.85	30.87	26.98	30.16	30.45	30.14	30.21	<b>32.10</b>
12	30.20	31.50	33.31	27.97	31.69	33.22	32.71	32.65	<b>34.64</b>
13	26.18	26.69	26.98	25.14	27.97	26.49	26.42	26.62	<b>28.30</b>
14	27.86	29.07	29.87	26.67	29.21	29.36	29.14	29.30	<b>31.18</b>
15	29.91	31.58	33.13	28.04	31.17	33.22	32.34	32.36	<b>34.27</b>
16	29.29	30.35	31.54	27.46	32.18	31.34	31.05	31.21	<b>33.72</b>
17	29.50	31.09	32.52	27.81	32.80	32.09	32.00	31.85	<b>33.61</b>
18	27.72	28.74	29.36	26.57	28.63	28.88	28.76	28.89	<b>30.56</b>
19	28.98	30.18	31.35	27.25	29.79	31.34	30.77	30.95	<b>33.10</b>
20	30.63	31.78	33.27	27.89	29.52	33.00	32.55	32.58	<b>34.18</b>
21	28.50	29.58	30.54	26.86	30.99	30.02	30.03	30.03	<b>31.69</b>
22	28.61	29.78	30.82	27.19	30.50	30.47	29.82	30.10	<b>32.08</b>
23	30.60	32.66	35.06	28.17	32.82	34.72	34.37	33.94	<b>35.16</b>
24	27.97	28.81	29.61	26.01	30.75	29.47	29.35	29.39	<b>30.93</b>
Average	28.92	30.19	31.44	27.04	30.73	31.17	30.91	30.89	<b>32.67</b>

350 

### 3. More visual comparisons of denoised images on the real noisy images of dataset [1]

 404  
351

352 In this section, we give more comparisons of the state-of-the-art denoising methods on dataset [1]. The real noisy images in  
353 dataset [1] have no “ground truth” images and hence we only compare the visual quality of the denoised images by different  
354 methods. As can be seen from Figures 7-10, the proposed MC-WNNM method performs better than the competing methods.

355 

### 4. More visual comparisons of denoised images on the real noisy images of dataset [2]

 409  
356

357 In this section, we provide more comparisons of the proposed method with the state-of-the-art denoising methods on the  
358 15 cropped real noisy images used in [2]. In this dataset, each scene was shot 500 times under the same camera and camera  
359 setting. The mean image of the 500 shots is roughly taken as the “ground truth”, with which the PSNR can be computed.  
360 As can be seen from Figures 11-14, our proposed method achieves better performance than the the competing methods. This  
361 validates the effectiveness of the proposed MC-WNNM method for real noisy image denoising.

432  
433  
434  
435  
436  
437  
438  
439  
440441  
442  
443  
444  
445  
446  
447  
448  
449  
450451  
452  
453  
454  
455  
456  
457  
458  
459  
460  
461  
462463  
464  
465  
466  
467  
468  
469  
470  
471  
472  
473474  
475  
476  
477  
478  
479  
480  
481  
482  
483  
484  
485486  
487  
488  
489  
490  
491  
492  
493  
494  
495  
496  
497  
498  
499  
500  
501  
502  
503  
504  
505506  
507  
508  
509  
510  
511  
512  
513  
514  
515  
516  
517518  
519  
520  
521  
522  
523  
524  
525  
526  
527528  
529  
530  
531  
532  
533  
534  
535  
536  
537  
538  
539

Figure 1. Denoised images of different methods on the image “kodim01” degraded by AWGN with different standard deviations of  $\sigma_r = 40$ ,  $\sigma_g = 20$ ,  $\sigma_b = 30$  on R, G, B channels, respectively. The images are better to be zoomed in on screen.

540  
541  
542  
543  
544  
545  
546  
547  
548594  
595  
596  
597  
598  
599  
600  
601  
602  
603  
604  
605  
606  
607  
608  
609  
610  
611  
612  
613549  
550  
551  
552  
553  
554  
555  
556  
557  
558603  
604  
605  
606  
607  
608  
609  
610  
611  
612  
613

559

614

560  
561  
562  
563  
564  
565  
566  
567  
568  
569  
570615  
616  
617  
618  
619  
620  
621  
622  
623  
624

571

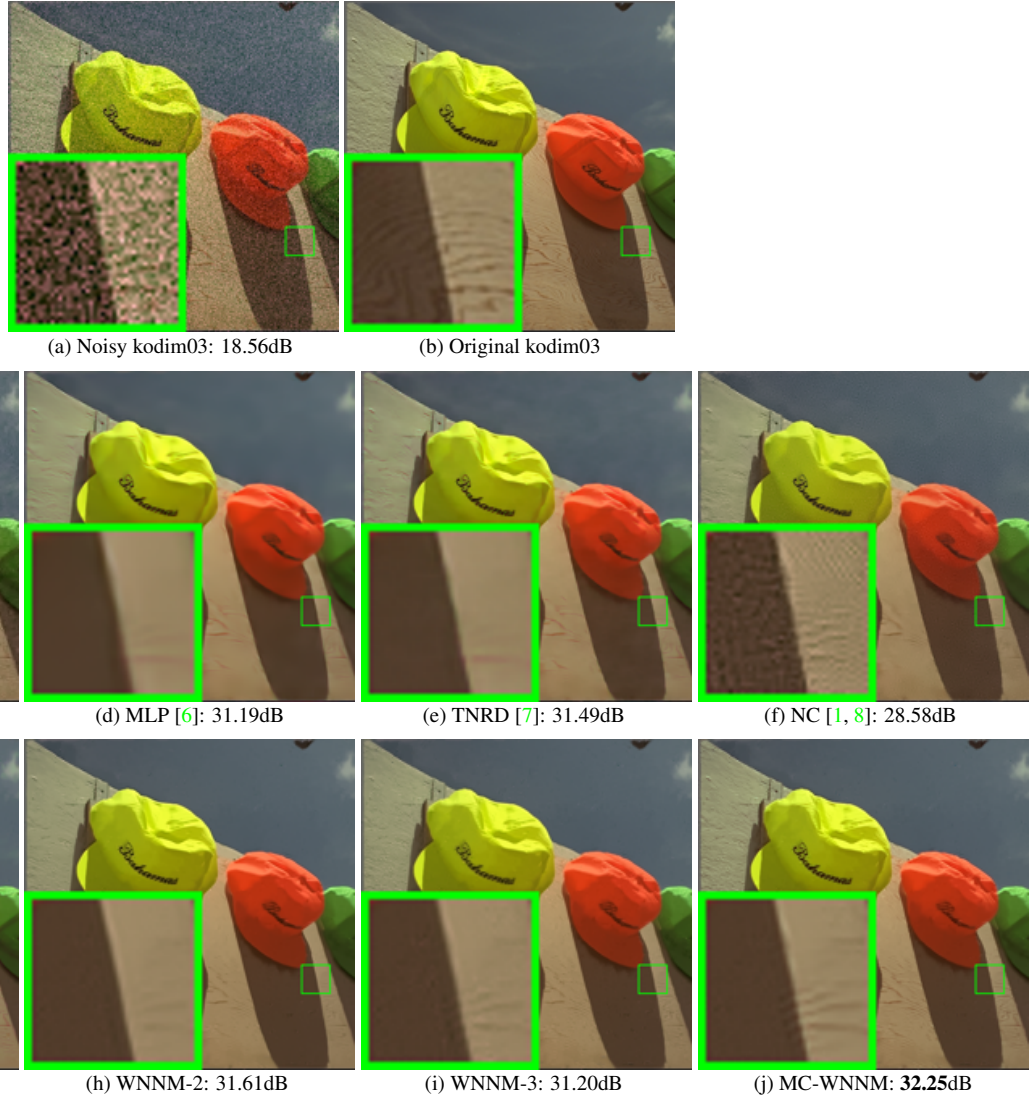
625  
626  
627  
628  
629  
630  
631  
632  
633  
634  
635572  
573  
574  
575  
576  
577  
578  
579  
580  
581636  
637  
638  
639  
640  
641  
642  
643  
644582  
583  
584  
585  
586  
587  
588  
589  
590  
591  
592  
593645  
646  
647

Figure 2. Denoised images of different methods on the image “kodim03” degraded by AWGN with different standard deviations of  $\sigma_r = 40$ ,  $\sigma_g = 20$ ,  $\sigma_b = 30$  on R, G, B channels, respectively. The images are better to be zoomed in on screen.

648  
649  
650  
651  
652  
653  
654  
655  
656  
657  
658  
659  
660  
661  
662  
663  
664  
665  
666702  
703  
704  
705  
706  
707  
708  
709  
710  
711  
712  
713  
714  
715  
716  
717  
718  
719  
720  
721  
722  
723  
724  
725  
726  
727  
728  
729  
730  
731  
732  
733  
734  
735  
736  
737  
738  
739  
740  
741  
742  
743  
744  
745  
746  
747  
748  
749  
750  
751  
752  
753  
754  
755667  
668  
669  
670  
671  
672  
673  
674  
675  
676  
677  
678  
679  
680  
681  
682  
683  
684  
685  
686  
687  
688  
689  
690  
691  
692  
693  
694  
695  
696  
697  
698  
699  
700  
701

Figure 3. Denoised images of different methods on the image “kodim17” degraded by AWGN with different standard deviations of  $\sigma_r = 30$ ,  $\sigma_g = 10$ ,  $\sigma_b = 50$  on R, G, B channels, respectively. The images are better to be zoomed in on screen.

756

757

758

759

760

761

762

763

764

765

766

767

768

769

770

771

772

773

774

775

776

777

778

779

780

781

782

783

784

785

786

787

788

789

790

791

792

793

794

795

796

797

798

799

800

801

802

803

804

805

806

807

808

809

810

811

812

813

814

815

816

817

818

819

820

821

822

823

824

825

826

827

828

829

830

831

832

833

834

835

836

837

838

839

840

841

842

843

844

845

846

847

848

849

850

851

852

853

854

855

856

857

858

859

860

861

862

863



Figure 4. Denoised images of different methods on the image “kodim19” degraded by AWGN with different standard deviations of  $\sigma_r = 30$ ,  $\sigma_g = 10$ ,  $\sigma_b = 50$  on R, G, B channels, respectively. The images are better to be zoomed in on screen.

864  
865  
866  
867  
868  
869  
870  
871  
872  
873  
874  
875  
876  
877  
878  
879  
880  
881  
882  
883  
884  
885  
886  
887  
888  
889  
890  
891  
892  
893  
894  
895  
896  
897  
898  
899  
900  
901  
902  
903  
904  
905  
906  
907  
910  
911  
912  
913  
914  
915  
916  
917

918  
919  
920  
921  
922  
923  
924  
925  
926  
927  
928  
929  
930  
931  
932  
933  
934  
935  
936  
937  
938  
939  
940  
941  
942  
943  
944  
945  
946  
947  
948  
949  
950  
951  
952  
953  
954  
955  
956  
957  
958  
959  
960  
961  
962  
963  
964  
965  
966  
967  
968  
969  
970  
971

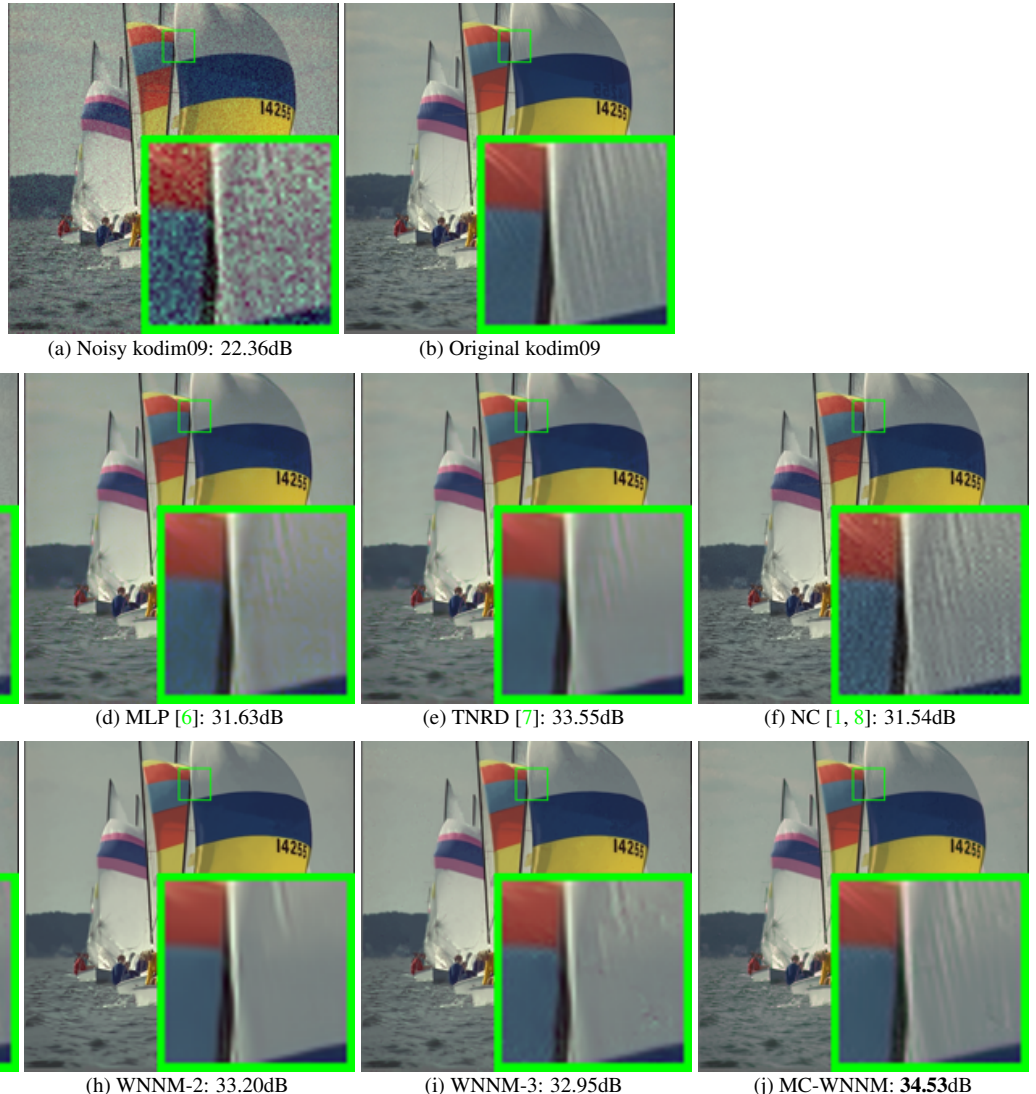


Figure 5. Denoised images of different methods on the image “kodim09” degraded by AWGN with different standard deviations of  $\sigma_r = 5$ ,  $\sigma_g = 30$ ,  $\sigma_b = 15$  on R, G, B channels, respectively. The images are better to be zoomed in on screen.

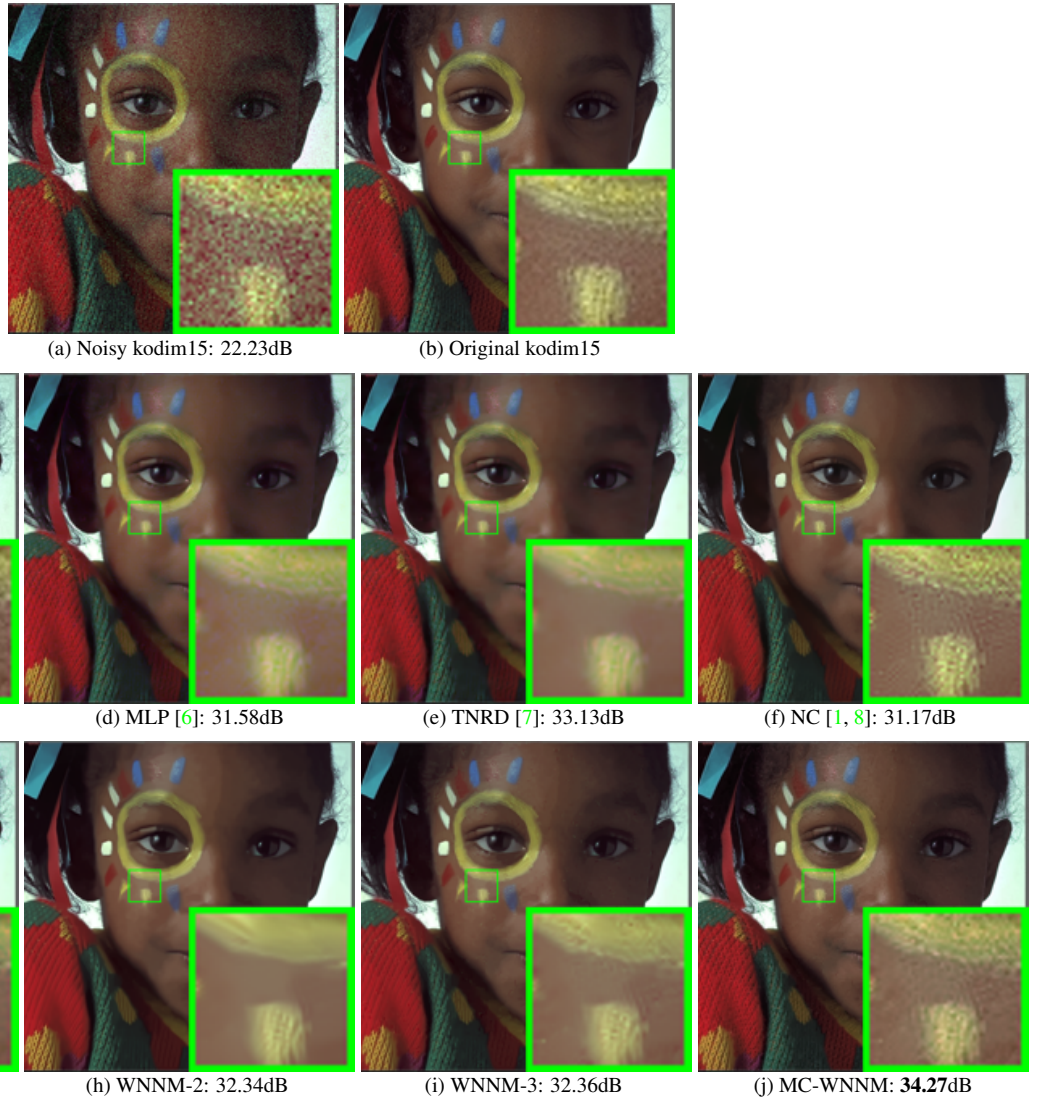


Figure 6. Denoised images of different methods on the image “kodim15” degraded by AWGN with different standard deviations of  $\sigma_r = 5$ ,  $\sigma_g = 30$ ,  $\sigma_b = 15$  on R, G, B channels, respectively. The images are better to be zoomed in on screen.

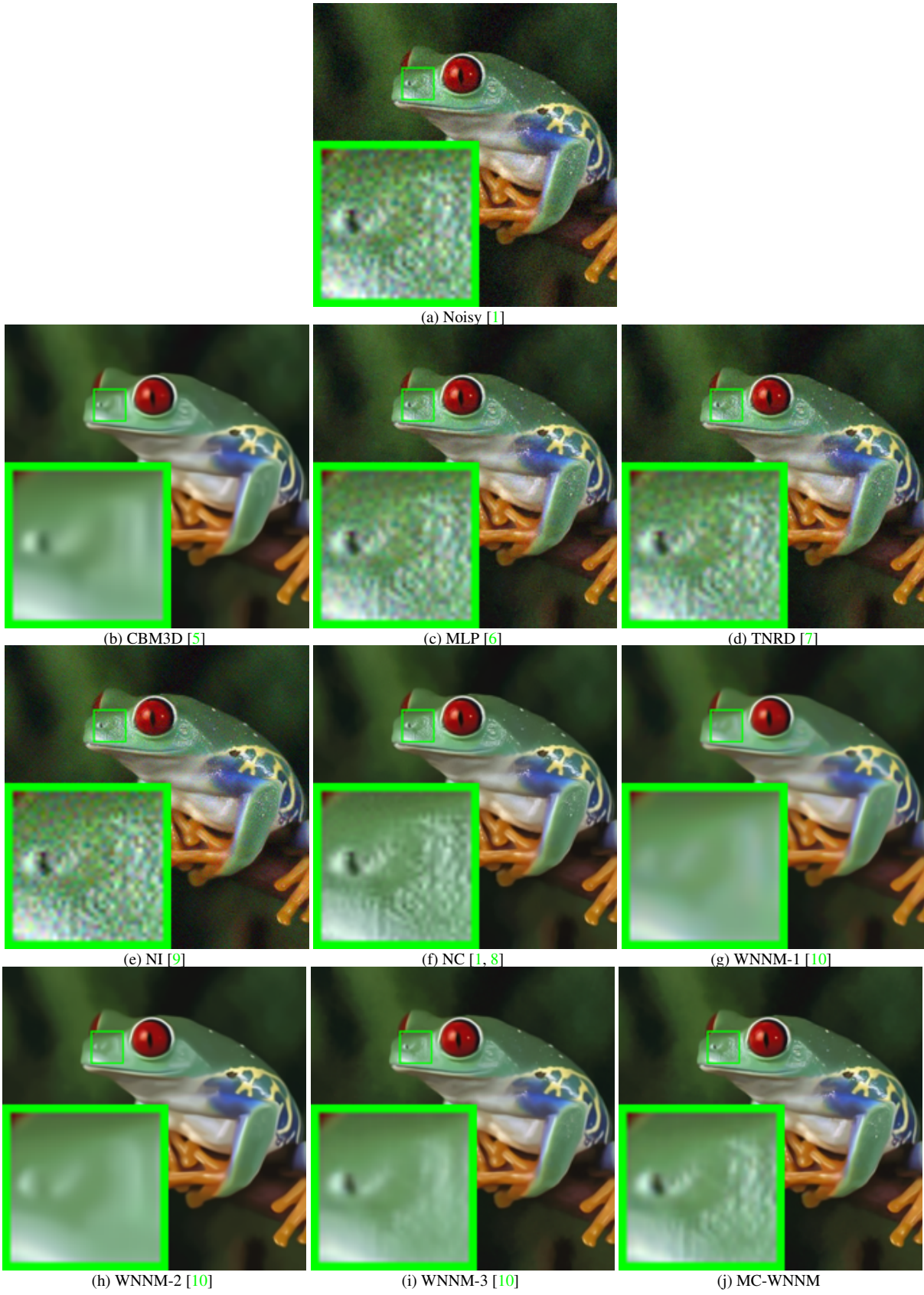


Figure 7. Denoised images of the real noisy image “Frog” [1] by different methods. The images are better to be zoomed in on screen.

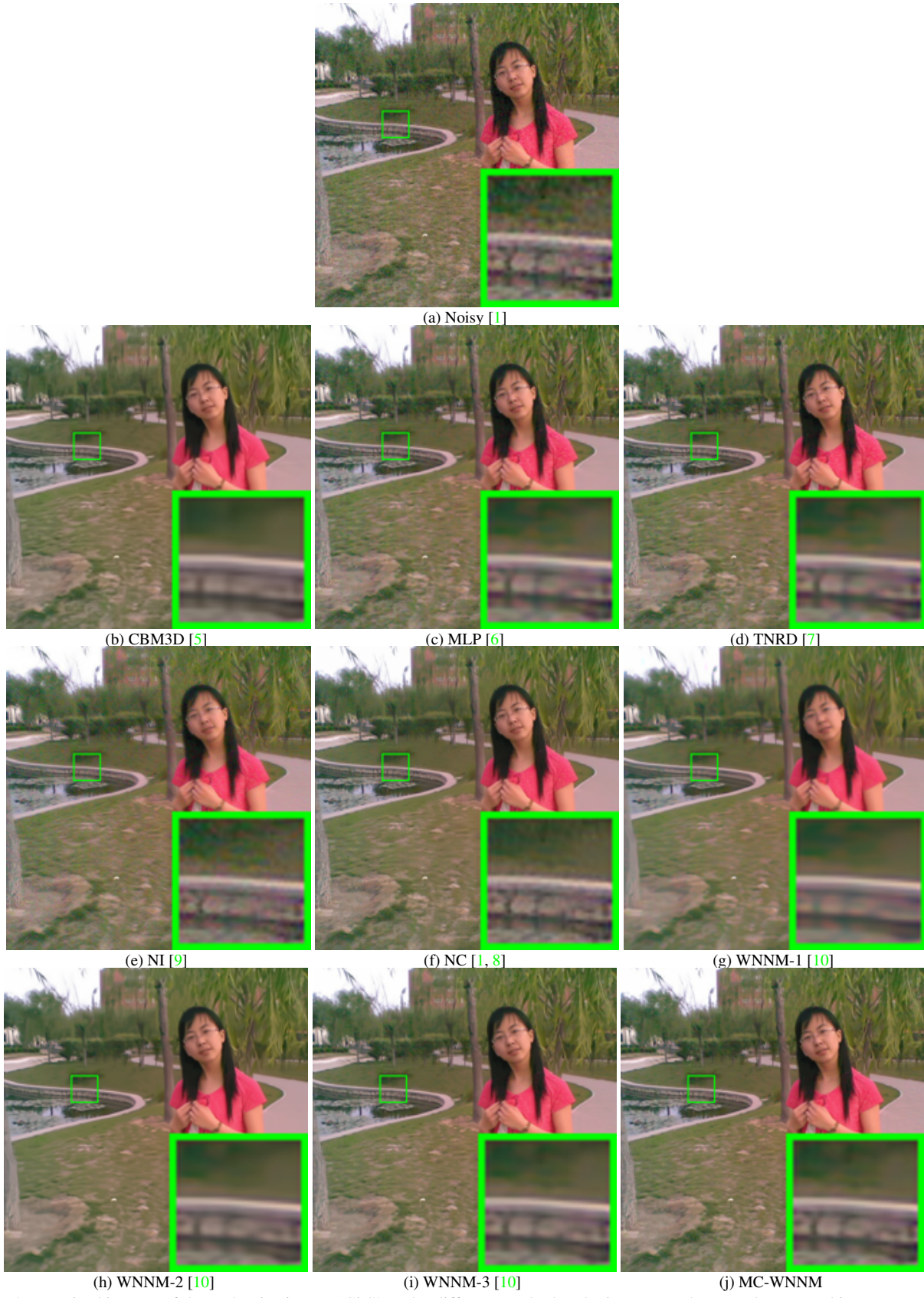
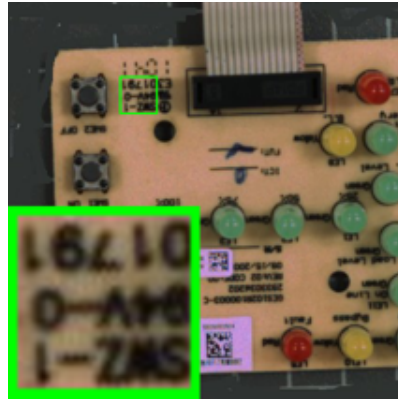


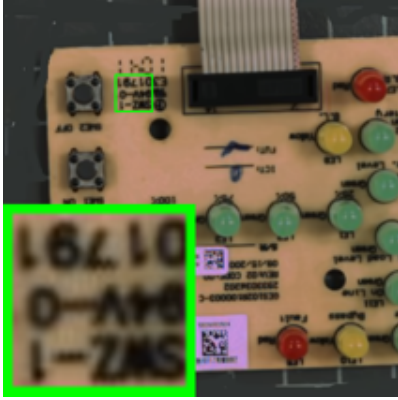
Figure 8. Denoised images of the real noisy image "Girl" [1] by different methods. The images are better to be zoomed in on screen.

1296  
1297  
1298  
1299  
1300  
1301  
1302  
1303  
1304  
1305  
1306  
1307  
1308

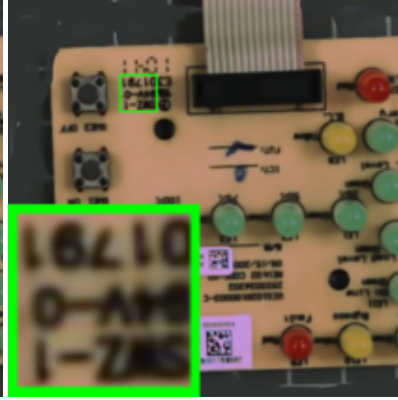
1350  
1351  
1352  
1353  
1354  
1355  
1356  
1357  
1358  
1359  
1360  
1361  
1362



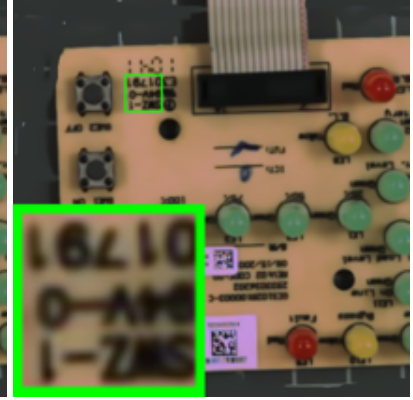
(a) Noisy [1]



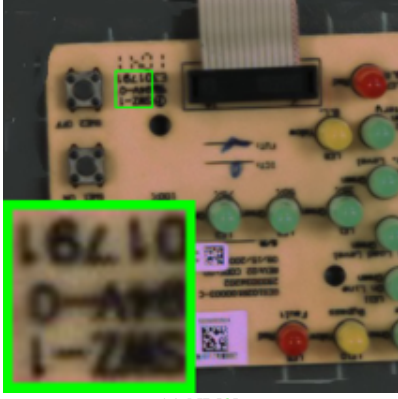
(b) CBM3D [5]



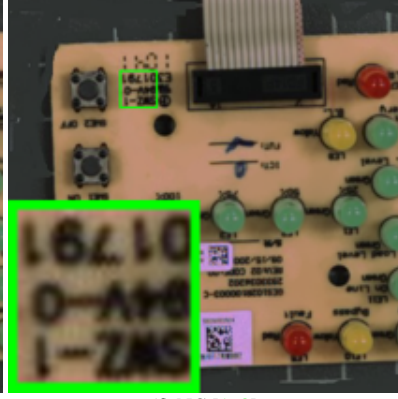
(c) MLP [6]



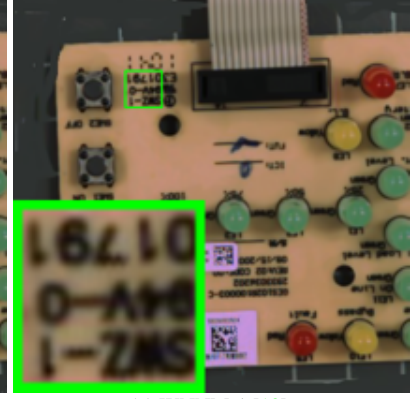
(d) TNRD [7]



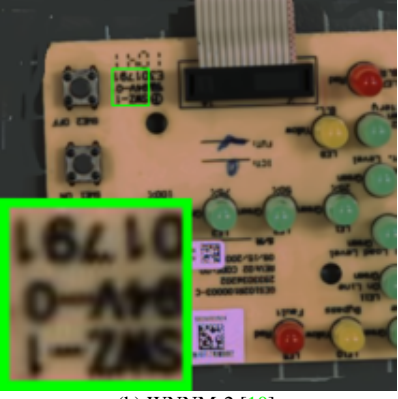
(e) NI [9]



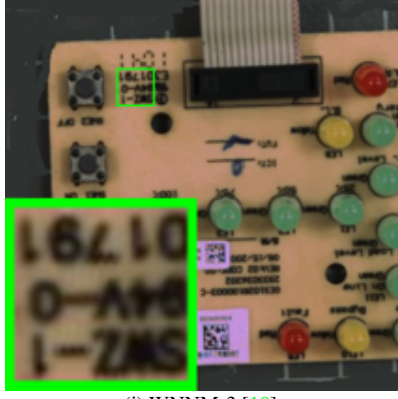
(f) NC [1, 8]



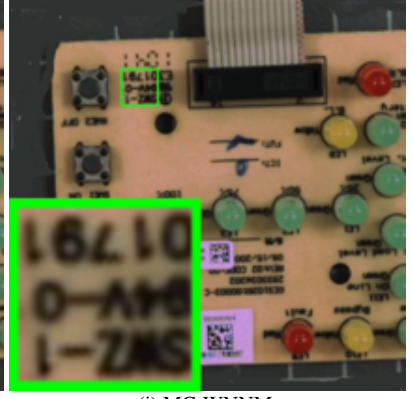
(g) WNNM-1 [10]



(h) WNNM-2 [10]



(i) WNNM-3 [10]



(j) MC-WNNM

1348

1402

Figure 9. Denoised images of the real noisy image “Circuit” [1] by different methods. The images are better to be zoomed in on screen.

1403

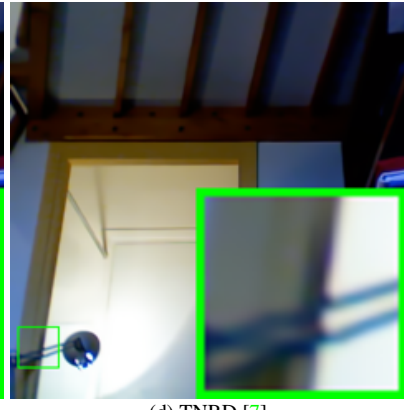
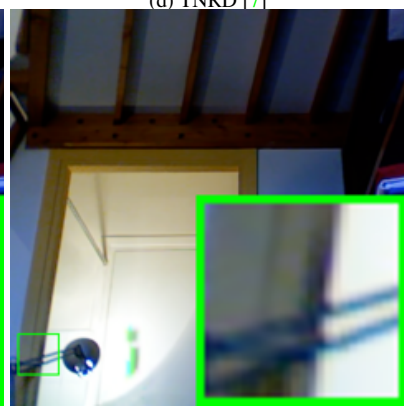
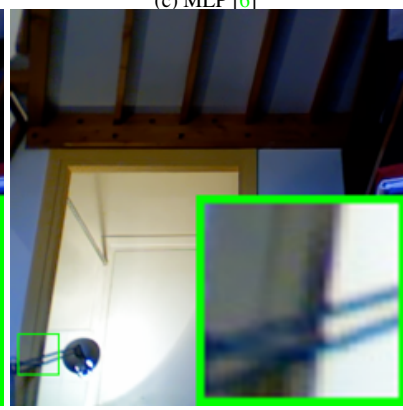
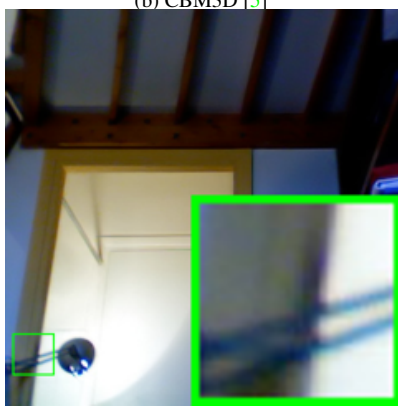
1404  
1405  
1406  
1407  
1408  
1409  
1410  
1411  
1412  
1413  
1414  
1415  
14161458  
1459  
1460  
1461  
1462  
1463  
1464  
1465  
1466  
1467  
1468  
1469  
14701417  
1418  
1419  
1420  
1421  
1422  
1423  
1424  
1425  
1426  
1427  
1428  
14291471  
1472  
1473  
1474  
1475  
1476  
1477  
1478  
1479  
1480  
1481  
1482  
14831430  
1431  
1432  
1433  
1434  
1435  
1436  
1437  
1438  
1439  
1440  
1441  
14421484  
1485  
1486  
1487  
1488  
1489  
1490  
1491  
1492  
1493  
1494  
1495  
14961443  
1444  
1445  
1446  
1447  
1448  
1449  
1450  
1451  
1452  
1453  
1454  
1455  
14561497  
1498  
1499  
1500  
1501  
1502  
1503  
1504  
1505  
1506  
1507  
1508  
1509  
1510  
1511

Figure 10. Denoised images of the real noisy image “Room” [1] by different methods. The images are better to be zoomed in on screen.

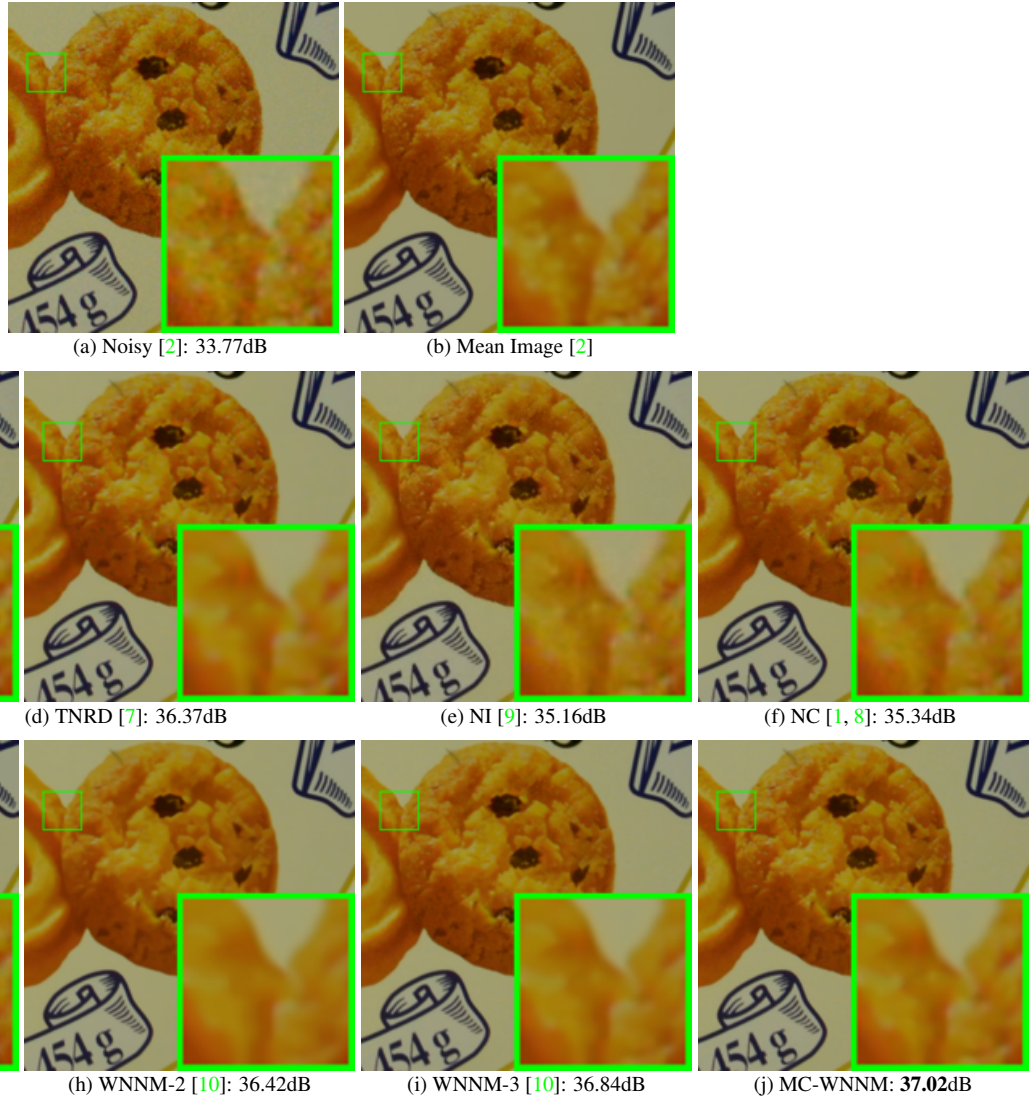


Figure 11. Denoised images of a region cropped from the real noisy image “Nikon D600 ISO 3200 2” [2] by different methods. The images are better to be zoomed in on screen.

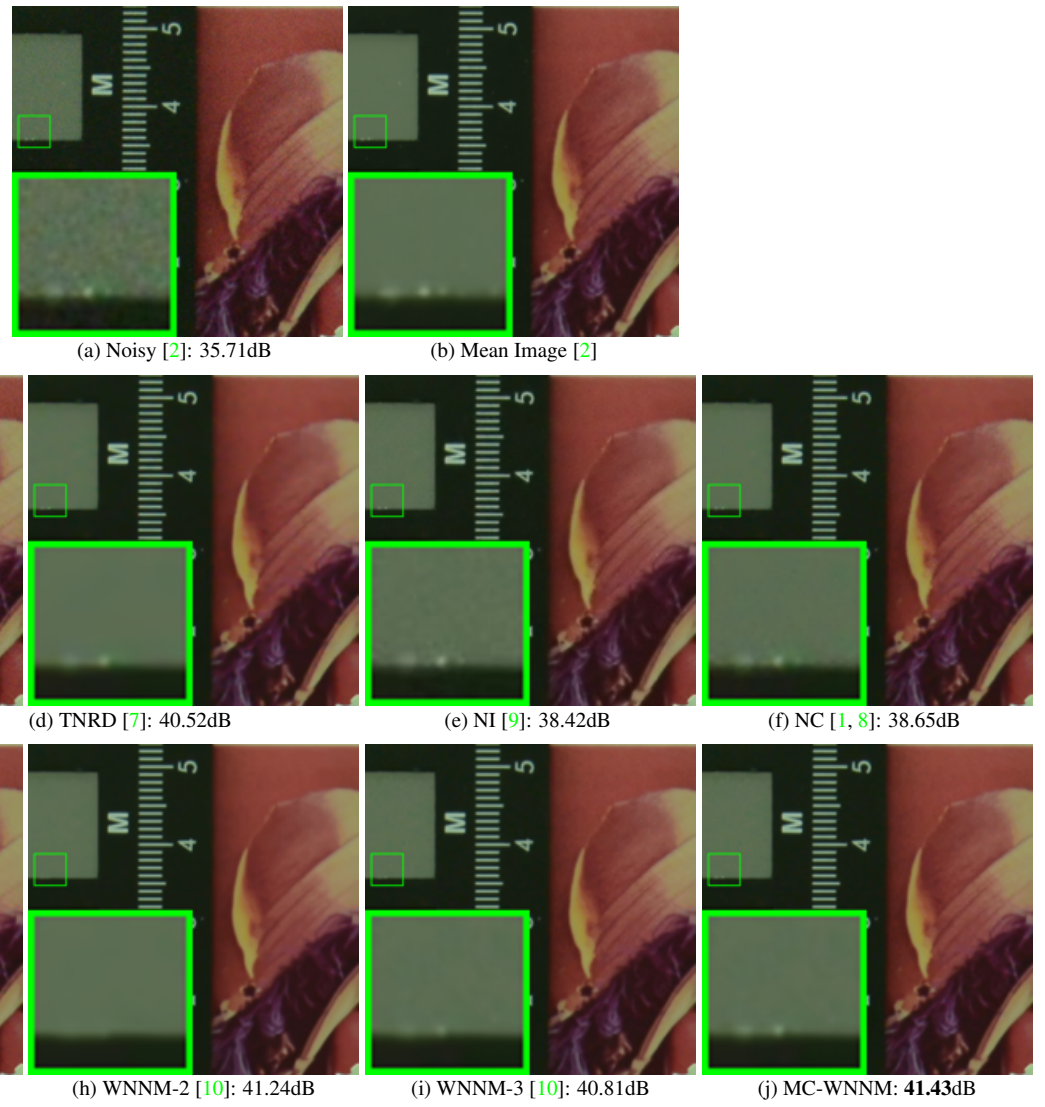


Figure 12. Denoised images of a region cropped from the real noisy image “Nikon D800 ISO 1600 2” [2] by different methods. The images are better to be zoomed in on screen.

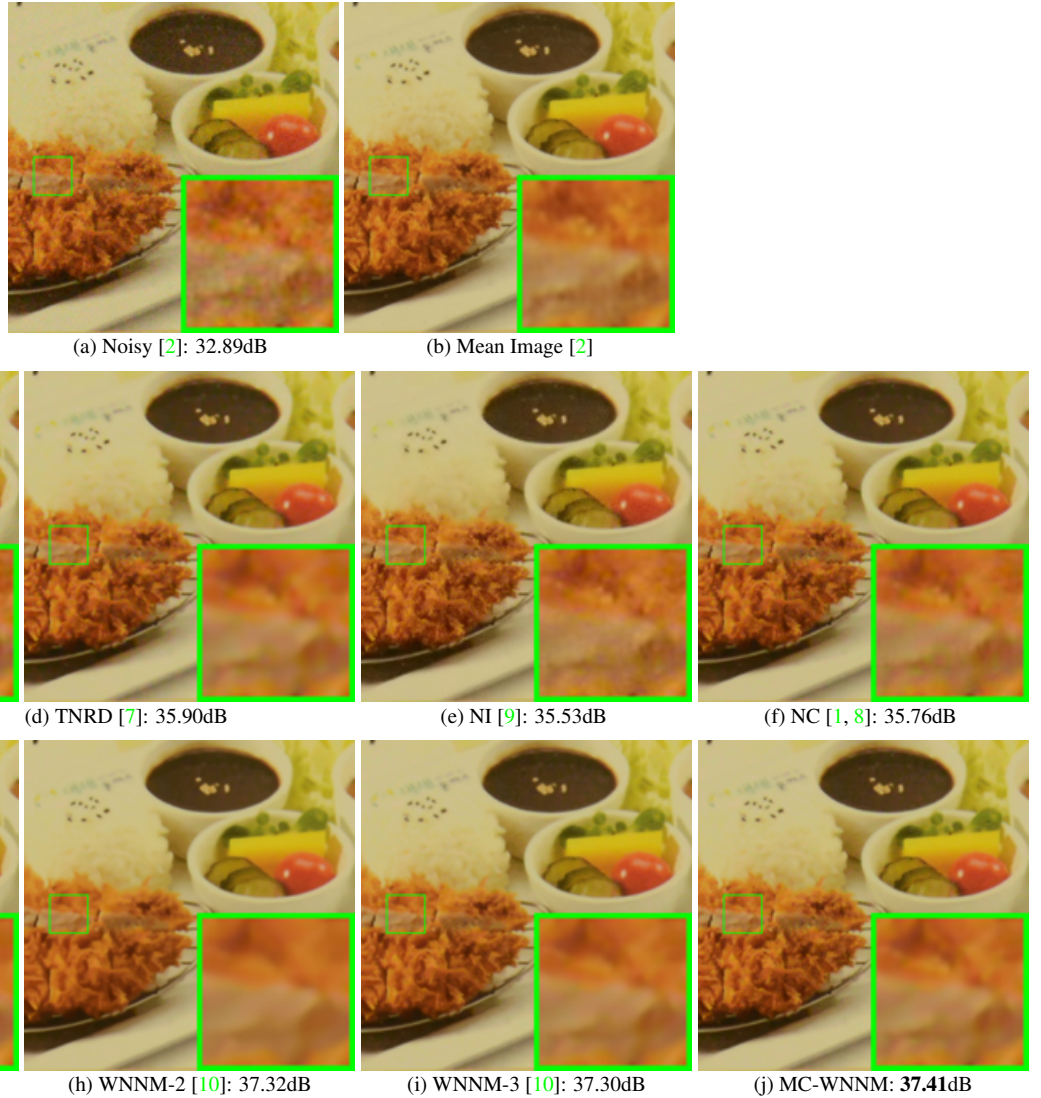


Figure 13. Denoised images of a region cropped from the real noisy image “Nikon D800 ISO 3200 2” [2] by different methods. The images are better to be zoomed in on screen.

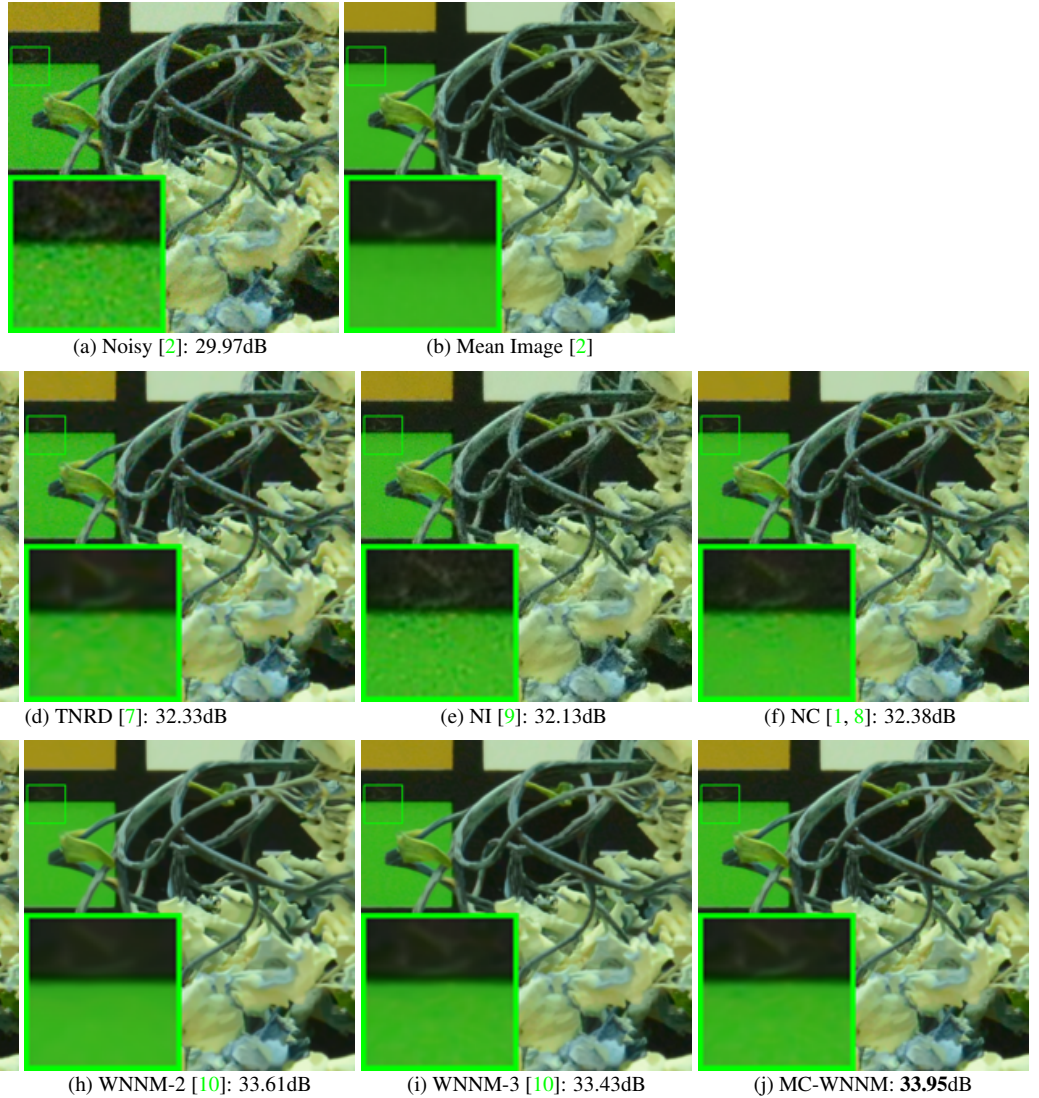


Figure 14. Denoised images of a region cropped from the real noisy image “Nikon D800 ISO 6400 2” [2] by different methods. The images are better to be zoomed in on screen.

1944 **References**

- 1945 1998  
1946 [1] M. Lebrun, M. Colom, and J. M. Morel. The noise clinic: a blind image denoising algorithm. [http://www.ipol.im/pub/  
1947 art/2015/125/](http://www.ipol.im/pub/art/2015/125/). Accessed 01 28, 2015. 1, 4, 5, 6, 7, 8, 9, 10, 11, 12, 13, 14, 15, 16, 17, 18 1999  
1948 2000  
1949 [2] S. Nam, Y. Hwang, Y. Matsushita, and S. J. Kim. A holistic approach to cross-channel image noise modeling and its application to 2001  
1950 image denoising. *IEEE Conference on Computer Vision and Pattern Recognition (CVPR)*, pages 1683–1691, 2016. 1, 4, 15, 16, 17, 18 2002  
1951 2003  
1952 [3] C. Eckart and G. Young. The approximation of one matrix by another of lower rank. *Psychometrika*, 1(3):211–218, 1936. 1 2004  
1953 2005  
1954 [4] S. Gu, Q. Xie, D. Meng, W. Zuo, X. Feng, and L. Zhang. Weighted nuclear norm minimization and its applications to low level 2006  
1955 vision. *International Journal of Computer Vision*, pages 1–26, 2016. 1 2007  
1956 [5] K. Dabov, A. Foi, V. Katkovnik, and K. Egiazarian. Color image denoising via sparse 3D collaborative filtering with grouping 2008  
1957 constraint in luminance-chrominance space. *IEEE International Conference on Image Processing (ICIP)*, pages 313–316, 2007. 5, 2009  
1958 6, 7, 8, 9, 10, 11, 12, 13, 14, 15, 16, 17, 18 2010  
1959 2011  
1960 [6] H. C. Burger, C. J. Schuler, and S. Harmeling. Image denoising: Can plain neural networks compete with BM3D? *IEEE Conference 2012  
1961 on Computer Vision and Pattern Recognition (CVPR)*, pages 2392–2399, 2012. 5, 6, 7, 8, 9, 10, 11, 12, 13, 14 2013  
1962 2014  
1963 [7] Y. Chen, W. Yu, and T. Pock. On learning optimized reaction diffusion processes for effective image restoration. *IEEE Conference 2015  
1964 on Computer Vision and Pattern Recognition (CVPR)*, pages 5261–5269, 2015. 5, 6, 7, 8, 9, 10, 11, 12, 13, 14, 15, 16, 17, 18 2016  
1965 2017  
1966 [8] M. Lebrun, M. Colom, and J.-M. Morel. Multiscale image blind denoising. *IEEE Transactions on Image Processing*, 24(10):3149– 2018  
1967 3161, 2015. 5, 6, 7, 8, 9, 10, 11, 12, 13, 14, 15, 16, 17, 18 2019  
1968 2020  
1969 [9] Neatlab ABSoft. Neat Image. <https://ni.neatvideo.com/home>. 11, 12, 13, 14, 15, 16, 17, 18 2021  
1970 2022  
1971 [10] S. Gu, L. Zhang, W. Zuo, and X. Feng. Weighted nuclear norm minimization with application to image denoising. *IEEE Conference 2023  
1972 on Computer Vision and Pattern Recognition (CVPR)*, pages 2862–2869, 2014. 11, 12, 13, 14, 15, 16, 17, 18 2024  
1973 2025  
1974 2026  
1975 2027  
1976 2028  
1977 2029  
1978 2030  
1979 2031  
1980 2032  
1981 2033  
1982 2034  
1983 2035  
1984 2036  
1985 2037  
1986 2038  
1987 2039  
1988 2040  
1989 2041  
1990 2042  
1991 2043  
1992 2044  
1993 2045  
1994 2046  
1995 2047  
1996 2048  
1997 2049  
1998 2050  
1999 2051